Structural, electrical and magnetic properties of cobalt ferrite with Nd^{3+} doping

Regaty Anitha Reddy, Kattepogu Rama Rao, Bitra Rajesh Babu, Guthikonda Kiran Kumar* , **Cherukupalli Rajesh, Anindita Chatterjee, Nadella Krishna Jyothi**

Abstract A systematic study on the influence of Nd^{3+} substitution on structural, magnetic and electrical properties of cobalt ferrite nanopowders obtained by sol–gel auto-combustion route was reported. The formation of spinel phase was confirmed by X-ray diffraction (XRD) data, and percolation limit of Nd^{3+} into the spinel lattice was also observed. Fourier transform infrared spectroscopy (FTIR) bands observed ≈ 580 and ≈ 390 cm^{-1} support the presence of Fe^{3+} at A and B sites in the spinel lattice. The variation in microstructure was investigated by scanning electron microscopy (SEM), and the average grain size varies from 5.3 to 3.3 µm. The substitution of Nd^{3+} significantly affects the formation of pores and grain size of cobalt ferrite. Room-temperature saturation magnetization and coercivity decrease from 60 to 30 mA·m^2·g^{-1} and 19.9–17.8 mT, respectively, with Nd^{3+} substitution increasing. These decreases in magnetic properties are explained based on the presence of non-magnetic nature of Nd^{3+} concentration and the dilution of super-exchange interaction in the spinel lattice. The room-temperature direct-current electrical resistivity increases with Nd^{3+} concentration increasing, which is due to the unavailability of Fe^{2+} at octahedral B sites.

Keywords Co-Nd ferrite; Saturation magnetization; DC resistivity

R. A. Reddy, N. K. Jyothi
Department of Physics, Koneru Lakshmaiah Education
Foundation, Vaddeswaram, Guntur, Andhra Pradesh 522502,
India

K. R. Rao
Department of Physics, Andhra University, Visakhapatnam,
Andhra Pradesh 530003, India

B. Rajesh Babu
Department of Physics, G.V.P. College of Engineering for
Women, Visakhapatnam, Andhra Pradesh 530048, India

G. K. Kumar*
Department of Physics, Raghu College of Engineering (A),
Bheemunipatnam, Visakhapatnam, Andhra Pradesh 531162,
India
e-mail: gkiran.phy@gmail.com

Ch. Rajesh
Department of Physics, Gayatri Vidya Parishad College of
Engineering (Autonomous), Visakhapatnam, Andhra Pradesh
530048, India

A. Chatterjee
Department of Chemistry, Raghu College of Engineering (A),
Bheemunipatnam, Visakhapatnam, Andhra Pradesh 531162,
India

1 Introduction

In recent years, among the family of spinel ferrites, cobalt ferrite has been rigorously investigated due to its tremendous applications in high-density magnetic recording media, microwave devices, high-sensitivity sensor and biomedical industries [1–4]. Apart from the promising electronic applications, they are also suitable and widely used in environmental remediation applications due to their excellent physical and chemical properties like high saturation magnetization, low cost, size- and shape-dependent and catalytic properties [5, 6].

The structural, electrical, magnetic and dielectric properties of cobalt ferrite are governed by the factors like method of preparation, sintering time and temperature, chemical composition, type and concentration of dopant. The spinel unit cell consists of cubic closed-pack arrangement of oxygen ions with 64 tetrahedral (A) and 32 octahedral interstitial sites (B). Out of these 96 interstitial

sites, only 8 and 16 cations are occupied in A and B sites, respectively, which are aligned in a mutually opposite direction. Thus, there is a great probability to tune the properties of the cobalt ferrite by rearranging the cations present in A and B sites. This is because magnetic and electrical properties are predominantly depending on cationic and charge distribution. Introducing a fraction of magnetic or non-magnetic ions with different valency states in the spinel ferrite affects significantly its structure, which further plays a crucial role in tuning its physical properties for various industrial applications. The rare-earth ions have unpaired 4f electrons, and they have a strong spin–orbit coupling. The substitution of rare-earth ions with Fe^{3+} site will cause 4f–3d coupling which is helpful to determine magneto-crystalline anisotropy of the material; therefore, it is possible to develop a magnetic core useful for low- and high-frequency applications. Several authors reported that substitution of rare-earth ions enhances the electromagnetic characteristics of the cobalt ferrite. Nikumbh et al. [7] reported decrease in magnetic parameters due to the substitution of Nd^{3+}, Sm^{3+} and Gd^{3+} in cobalt ferrite. On the other hand, Tahmineh et al. [8] and Dascalu et al. [9] observed that Tb^{3+} could enhance the saturation magnetization of cobalt ferrite and make it a suitable candidate for recording head applications. Thus, the objective of the present study is to investigate the influence of Nd^{3+} doping on structural, electrical and magnetic properties of cobalt ferrite system. Moreover, due to the larger ionic radii of Nd^{3+}, it requires higher energy to enter into the spinel lattice. Therefore, standard ceramic route has been chosen in the present work and it is expected that they must occupy the larger B sites, which produce an unusual magnetic behavior upon Nd^{3+} substitution.

2 Experimental

Neodymium (Nd^{3+})-substituted cobalt ferrite with chemical composition $CoNd_xFe_{2-x}O_4$ (x = 0, 0.010, 0.015, 0.020, 0.025, 0.030) was synthesized by standard ceramic method. High-purity analytical-grade (analytical reagent (AR)) precursors of CoO (99.9%), Fe_2O_3 (99.9%) and NdO(99.9%) were used as starting materials in desired stoichiometric proportions. The starting precursors were weighed and mixed thoroughly in agate motor and calcined at 1173 K for 4 h. These powders were compacted in the form of pellets by adding 5% polyvinyl alcohol (PVA) as a binder. Finally, the powder materials and pellets were sintered again at 1473 K for 4 h followed by natural cooling to room temperature. The sintered samples are subjected to various characterization techniques to understand the modifications in structural, electrical and magnetic properties as a function of Nd^{3+} concentration.

Cobalt ferrite powders were analyzed to identify the phase formation by using Panalytical X'Pert Pro MPD X-ray diffractometer (XRD) with Cu Kα radiation (λ = 0.154056 nm) in the range of 10°–80°. The infrared spectra were recorded in the range of 4000–400 cm^{-1} with Shimadzu Fourier transform infrared spectroscopy (FTIR) Prestige-21. Microstructural changes were studied using LEO 435 VP scanning electron microscope (SEM). Prior to scanning, surfaces of the pellets were coated with a thin layer of platinum. The magnetization measurement was carried out by LAKESHORE VSM-7410 vibrating sample magnetometer (VSM) with maximum applied field of 2 T at room temperature. The room-temperature direct-current (DC) electrical resistivity measurements were done on the disk-shaped pellets using standard two-probe method at a small electric field of 1 V·cm^{-1} for all samples.

3 Results and discussion

3.1 XRD results

XRD patterns of $CoNd_xFe_{2-x}O_4$ (x = 0, 0.010, 0.015, 0.020, 0.025, 0.030) samples are shown in Fig. 1. It is clear from that all the samples exhibit cubic spinel phase, and prominent peaks corresponding to (220), (311), (222), (400), (422), (511) and (440) planes are in accordance with standard JCPDS card No. 22-1086. The lattice constant a was calculated according to the following equation:

$$a_{exp} = d\sqrt{h^2 + k^2 + l^2} \tag{1}$$

where d is the inter-planar distance of each plane and (hkl) are Miller indices. Nelson–Riley extrapolation method was used to find the accurate lattice constant, as listed in
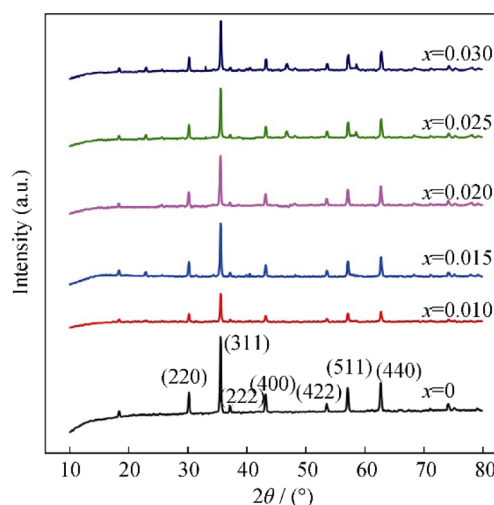
Fig. 1 XRD patterns of $CoNd_xFe_{2-x}O_4$ (x = 0, 0.010, 0.015, 0.020, 0.025, 0.030) samples

Table 1 Average crystallite size, X-ray density, FTIR frequency band positions (ν_1 and ν_2) and grain size of $CoNd_xFe_{2-x}O_4$ ($x = 0$, 0.010, 0.015, 0.020, 0.025, 0.030) samples

x	Lattice constant/nm	Crystallite size D_{311}/nm	Density/gm·cm^{-3}	ν_1/cm^{-1}	ν_2/cm^{-1}	Grain size/μm
0	0.83699	49	4.61	388	579	5.3
0.010	0.83714	48	4.63	397	581	3.3
0.015	0.83722	51	4.65	393	583	6.4
0.020	0.83729	52	4.67	384	581	5.3
0.025	0.83719	53	4.69	384	583	4.4
0.030	0.83707	46	4.70	395	583	4.2

Table 1 [10]. It is clear from Table 1 that lattice constant increases linearly with Nd^{3+} and then decreases when $x > 0.02$. The observed increase is due to the replacement of Fe^{3+} (0.065 nm) at B site by larger ionic radii Nd^{3+} (0.0995 nm). Similar variation in lattice constant with Nd^{3+} substitution in different ferrite systems has been reported in studies [11, 12]. However, the decrease in lattice constant for the composition $x \geq 0.020$ is ascribed to the possible diffusion of Nd^{3+} to the grain boundaries instead of entering into the lattice site. Therefore, the percolation limit of Nd^{3+} concentration to accommodate into the octahedral spinel lattice is 0.02 mol %. Hameda et al. [13] and Farid et al. [14] observed similar variation in lattice constant in their investigation with Nd^{3+} substitution. The average crystallite size for all the samples was calculated using the following Debye–Scherer's equation, as listed in Table 1:

$$D_{311} = \frac{0.9\lambda}{\beta \cos \theta} \tag{2}$$

where D_{311}, λ, β and θ are volume-averaged crystallite size, wavelength of X-ray (0.15406 nm), full width at half maximum of (311) peak and diffraction angle, respectively. The average crystallite size varies randomly with Nd^{3+} content increasing between 46 and 49 nm. The calculated X-ray density (d_x) of all the samples was calculated by the following formula:

$$d_x = \frac{ZM_w}{N_A V_C} \tag{3}$$

where Z is the number of formula units in a unit cell, M_w is the molecular weight of the sample, N_A is the Avogadro's number and V_C is volume of the cell. From Table 1, a linear dependence of X-ray density on Nd^{3+} concentration is observed. This variation in density is a direct consequence of higher molecular weight of Nd^{3+} than Fe^{3+} concentration. It is worthwhile to mention the influence of large ionic radii on hoping lengths of spinel lattice. The following equations were used to calculate the tetrahedral hopping length (L_A) and octahedral hopping length (L_B):

$$L_A = \frac{1}{4}a\sqrt{3} \text{ and } L_B = \frac{1}{4}a\sqrt{2} \tag{4}$$

Figure 2 shows the composition dependence of hoping lengths at A and B sites. It can be observed that hopping lengths follow the similar trend with that of lattice constant, suggesting the increase in the distance between the ions in the respective sublattice. The separation between the ions due to the substitution of larger Nd^{3+} modifies the magnetic and electrical properties.

3.2 FTIR and microstructure study

Infrared spectra of Nd^{3+}-substituted cobalt ferrite are shown in Fig. 3. Two prominent absorption bands in the range of 350–400 and 550–600 cm^{-1} are noticed. The high-frequency absorption band ν_1 corresponds to the stretching vibration of the octahedral metal oxygen bond, and low-frequency band ν_2 is due to the metal oxygen vibrations at tetrahedral sites. The positions of the bands are listed in Table 1. Both tetrahedral and octahedral band positions are shifted to higher frequency side. The shift in band positions is due to the variation in $Fe^{3+} \leftrightarrow O^{2-}$ bond length and cation redistribution. In the present work, occupation of Nd^{3+} in octahedral B site with larger ionic radii is responsible for the observed shift in absorption bands. It is also observed from Fig. 3 that broadening of ν_2
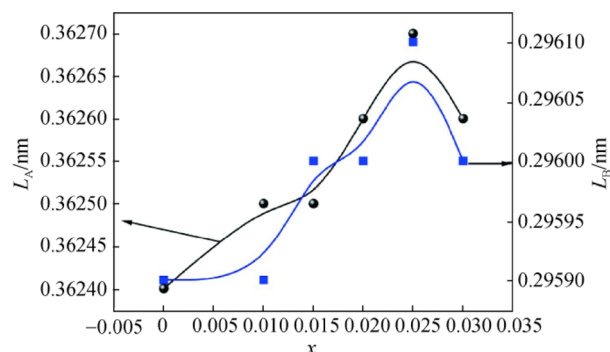
Fig. 2 Hopping lengths (L) of $CoNd_xFe_{2-x}O_4$ ($x = 0$, 0.010, 0.015, 0.020, 0.025, 0.030) samples
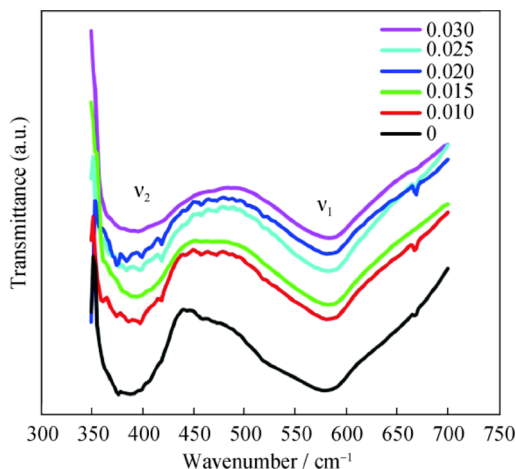
Fig. 3 FTIR spectra of $CoNd_xFe_{2-x}O_4$ ($x = 0$, 0.010, 0.015, 0.020, 0.025, 0.030) samples

band increases with Nd^{3+} concentration increasing, which suggests the occupancy of Nd^{3+} on octahedral B sites [15].
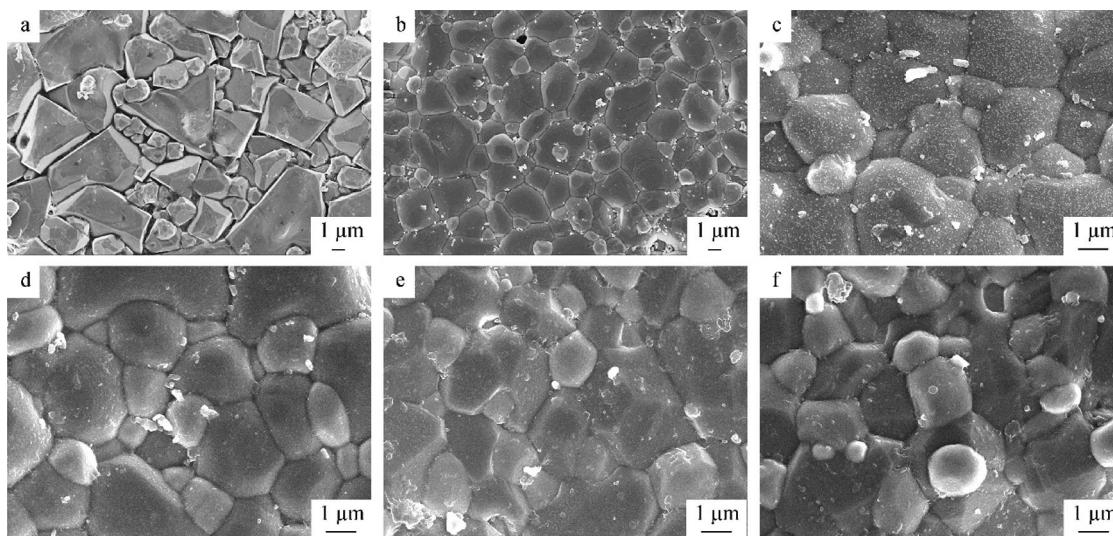
The typical SEM images of $CoNd_xFe_{2-x}O_4$ ($x = 0$, 0.010, 0.015, 0.020, 0.025, 0.030) are presented in Fig. 4. It is well known that grain size and structure influence the physical properties of ferrites. Grain growth is closely related to the grain boundary mobility, because there is a competition between the driving force for grain boundary movement and the retarding force exerted by the pores during the grain growth [16]. The grain size is calculated using linear intercept method and presented in Table 1. It is to be noted that the addition of Nd^{3+} significantly impedes the grain growth. The observed variations in grain size and formation of secondary phase are consistent with reported results in the literature by various authors, but in different ferrite systems [17, 18].
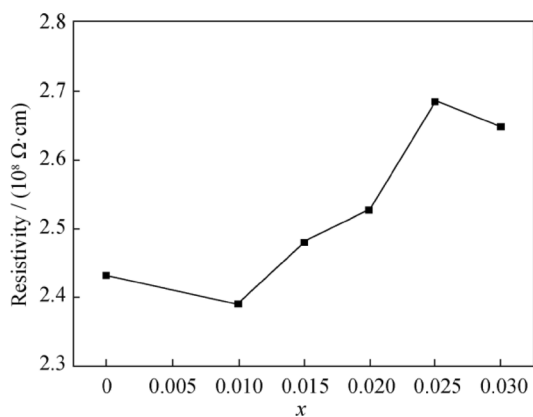
3.3 Electrical resistivity

The electrical properties of spinel ferrite are strongly influenced by the microstructure, availability of cations (Fe^{3+} and Fe^{2+}) and their distribution among A and B sites, which in turn depend on the synthesis processes and conditions. It can be seen from Fig. 5 that room-temperature (303 K) DC electrical resistivity increases with Nd^{3+} content increasing. It is known that conduction in spinals is due to the charge transfer of electrons between cations on B sites of different valences, because A–A hopping does not exist as there are only Fe^{3+} on this sublattice and any Fe^{2+} formed during processing preferentially occupy the B sites, and B–B hopping is more dominant than A–B hopping [19]. In the present work, substitution of Nd^{3+} at the expense of Fe^{3+} reduces the availability of ferric ions at B site. This in turn enhances the resistivity of the ferrite. However, hopping takes place among Fe^{2+} and Fe^{3+} due to the presence of secondary phase at grain boundaries. This may be responsible for the slight increment in the resistivity.

3.4 Magnetic properties

The magnetism of the spinel ferrite is due to the super-exchange coupling of uncompensated electron spins of the individual magnetic ions through oxygen ions. Owing to this super-exchange interaction, the spins are aligned antiparallel in the two (A and B) sublattices of spinel structure [20]. Therefore, the net magnetic moment is the difference between individual magnetic moments of A and B sublattice, i.e., $M = |M_B - M_A|$, where M_A and M_B are magnetic moment of ions residing at A and B sites, respectively. Figure 6 represents the hysteresis loops of

Fig. 4 SEM images of $CoNd_xFe_{2-x}O_4$: **a** $x = 0$, **b** $x = 0.010$, **c** $x = 0.015$, **d** $x = 0.020$, **e** $x = 0.025$ and **f** $x = 0.030$

Fig. 5 Room-temperature DC electrical resistivity of $CoNd_xFe_{2-x}O_4$ ($x = 0$, 0.010, 0.015, 0.020, 0.025, 0.030) samples
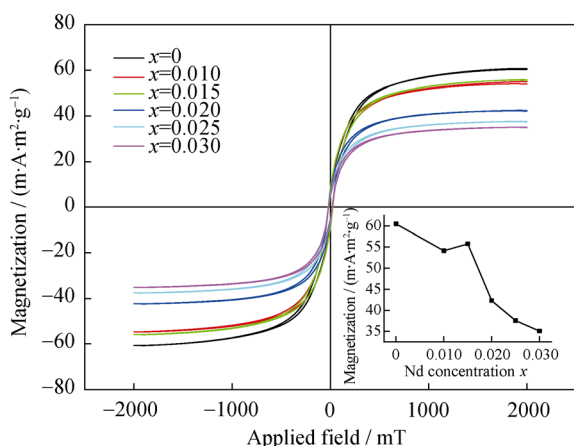
Fig. 6 Magnetic hysteresis loops for $CoNd_xFe_{2-x}O_4$ ($x = 0$, 0.010, 0.015, 0.020, 0.025, 0.030) samples and inset being variation of magnetization with Nd concentration

Nd^{3+}-substituted cobalt ferrite, which clearly shows the ferromagnetic behavior. From these plots (Fig. 6), the saturation magnetization (M_s), coercivity (H_c) and ratio of remanence to saturation magnetization (M_r/M_s) were calculated, as listed in Table 2. It is well known that the 4f electrons are responsible for the magnetic moment of rare-earth ions and their magnetic ordering temperature is effective at 40 K [21]. Therefore, the effect of Nd^{3+} on net

magnetic moment of spinel is almost negligible. However, due to their presence at octahedral (B) site, some of Fe^{3+} may shift to tetrahedral (A) site, which in turn alters the magnetic properties.

It is observed that as the concentration of Nd^{3+} increases, saturation magnetization (M_s) decreases. The value of M_s is seen to decrease from 60 $mA·m^2·g^{-1}$ for undoped cobalt ferrite to 35 $mA·m^2·g^{-1}$ for $CoNd_{0.03}Fe_{1.97}O_4$. The effective magnetic moment of Nd^{3+} is 3.2 μ_B, which is smaller than that of Fe^{3+} (5.0 μ_B). Therefore, substitution of Fe^{3+} by Nd^{3+} at B site causes M_s to decrease. In the present investigation, saturation magnetization values are higher than the reported values [22–24]. The coercivity decreases from 19.9 mT ($x = 0$) to 17.4 mT ($x = 0.030$) with Nd^{3+} content. This is due to the decrease in magnetic anisotropy of the system. The behavior of coercivity can be understood from Brown's relation given by:

$$H_c = \frac{2K_1}{\mu_0 M_s} \tag{5}$$

where K_1 is the magnetic anisotropy, μ_o is the permeability of free space and M_s is the saturation magnetization. According to the above relation, H_c is inversely proportional to M_s and directly related to K_1. It is reported that substitution of Nd^{3+} reduces the anisotropy constant [5, 18, 25]. The coercivity of the pure cobalt ferrite predominantly originated from the single-ion anisotropy of the octahedral Co^{2+}. Similar to Co^{2+}, Nd^{3+} also shows a strong spin–orbit coupling and contributes to the anisotropy, when they are located in the B sites of spinel ferrites. However, remarkable decrease in coercivity may be ascribed to the larger lattice distortion and smaller reduction in crystalline size. Therefore, for all samples, contribution of the anisotropy leads to the decrease in coercivity.

4 Conclusion

Nd^{3+}-substituted cobalt ferrite was synthesized using standard ceramic method, and its effects on structural,

Table 2 Saturation magnetization (M_s), coercivity (H_c), remanence magnetization (M_r) and magnetic moment (n_B) of $CoNd_xFe_{2-x}O_4$ ($x = 0$, 0.010, 0.015, 0.020, 0.025, 0.030) samples

x	$M_s/(mA·m^2·g^{-1})$	H_c/mT	$M_r/(mA·m^2·g^{-1})$	n_B (exp.)$/\mu_B$
0	60.4	19.9	7.31	2.20
0.010	54.1	23.1	8.92	2.06
0.015	55.8	19.6	7.21	2.17
0.020	42.3	17.6	6.35	1.68
0.025	37.5	17.8	5.51	1.52
0.030	35.1	17.4	4.98	1.45

electrical and magnetic properties were studied. XRD study shows the formation of single phase with cubic spinel structure. Crystallite size and grain size are affected by the substitution of Nd^{3+}, suggesting that growth of crystallite size is obstructed by the substitution of Nd^{3+}. The room-temperature DC electrical resistivity increases and saturation magnetization decreases with Nd^{3+} substitution increasing. Finally, it is concluded that the properties of cobalt ferrite get affected by changing parameters such as amount of substitution, method of processing, sintering temperature as well as cationic distribution and play a major role.

References

[1] Shirsath SE, Kadam RH, Mane ML, Ali G, Yasukawa Y, Liu XX, Morisako A. Permeability and magnetic interactions in Co^{2+} substituted $Li_{0.5}Fe_{2.5}O_4$ alloys. J Alloys Compd. 2013;575:145.

[2] Kishimoto M, Sakurai Y, Ajima T. Magneto-optical properties of Ba-ferrite particulate media. J Appl Phys. 1994;76(11):7506.

[3] Li F, Liu JJ, Evans DG, Duan X. Stoichiometric synthesis of pure MFe_2O_4 (M = Mg, Co, and Ni) spinel ferrites from tailored layered double hydroxide (hydrotalcite-like) precursors. Chem Mater. 2004;16(8):1597.

[4] Kasapoğlu N, Birsöz B, Baykal A, Köseoğlu Y, Toprak MS. Microwave-induced combustion synthesis and characterization of $Ni_xCo_{1-x}Fe_2O_4$ nanocrystals (x = 0, 0.4, 0.6, 0.8, 1.0). Central Eur J Chem. 2007;5(2):570–80.

[5] Hassani A, Eghbali P, Ekicibil A, Metin O. Monodisperse cobalt ferrite nanoparticles assembled on mesoporous graphitic carbon nitride ($CoFe_2O_4/mpg-C_3N_4$): a magnetically recoverable nanocomposite for the photocatalytic degradation of organic dyes. J Magn Magn Mater. 2018;456:400.

[6] Hassani A, Çelikdağ G, Eghbali P, Sevim M, Karaca S, Metin O. Heterogeneous sono-Fenton-like process using magnetic cobalt ferrite-reduced graphene oxide ($CoFe_2O_4$-rGO) nanocomposite for the removal of organic dyes from aqueous solution. Ultra Sonochem. 2018;40:841.

[7] Nikumbh AK, Pawar RA, Nighot DV, Gugale GS, Sangale MD, Khanvilkar MB, Nagawade AV. Structural, electrical, magnetic and dielectric properties of rare-earth substituted cobalt ferrites nanoparticles synthesized by the co-precipitation method. J Magn Magn Mater. 2014;355:201.

[8] Sodaee T, Ghasemi A, Paimozd E. Remarkable influence of terbium cations on the magnetic properties of cobalt ferrite nanoparticles. Mater Phys Mech. 2013;17(1):11.

[9] Dascalu G, Chazallon GPB, Nica V, Caltun OF, Gurlui S, Focsa C. Rare earth doped cobalt ferrite thin films deposited by PLD. Appl Phys A. 2013;110(4):915–22.

[10] Nelson JB, Riley DP. An experimental investigation of extrapolation methods in the derivation of accurate unit-cell dimensions of crystals. Proc Phys Soc. 1945;57(3):160.

[11] Shinde TJ, Gadkari AB, Vasambekar PN. Effect of Nd^{3+} substitution on structural and electrical properties of nanocrystalline zinc ferrite. J Magn Magn Mater. 2010;322(18):2777.

[12] Fan XF, Ren HP, Zhang YH, Guo SH, Wang XL. Effects of Nd^{3+} on the microstructure and magnetic properties of Ni–Zn ferrites. Rare Met. 2008;27(3):287.

[13] Hameda OM, Said MZ, Barakat MM. Spectral and transport phenomena in Ni ferrite-substituted Gd_2O_3. J Magn Magn Mater. 2001;224(2):132.

[14] Farid MT, Ahmad I, Aman S, Kanwal M, Murtaza G, Ali I, Ahmad I, Ishfaq M. Structural, electrical and dielectric behavior of $Ni_xCo_{1-x}Nd_yFe_{2-y}O_4$ nano-ferrites synthesized by sol–gel method. Digest J Nanomater Biostruct. 2015;10:265.

[15] Shinde TJ, Gadkari AB, Vasambekar PM. Influence of Nd^{3+} substitution on structural, electrical and magnetic properties of nanocrystalline nickel ferrites. J Alloys Compd. 2012;513:80.

[16] Shinde TJ, Gadkari AB, Vsambekar PN. Saturation magnetization and structural analysis of $Ni_{0.6}Zn_{0.4}Nd_yFe_{2-y}O_4$ by XRD, IR and SEM techniques. J Mat Sci Mater Electron. 2010;21(2):120.

[17] Coasta ACFM, Mirelli MR, Kiminami RHGA. Combustion synthesis, sintering and magnetical properties of nanocristalline Ni–Zn ferrites doped with samarium. J Mater Sci. 2004;39(5):1773.

[18] Şabikoğlu I, Paral L, Malina O, Novak P, Kaslik J, Tucek J, Pechousek J, Navarik J, Schneeweiss O. The effect of neodymium substitution on the structural and magnetic properties of nickel ferrite. Prog Nat Sci Mater Int. 2015;25(3):215.

[19] El-Sayed AM. Electrical conductivity of nickel–zinc and Cr substituted nickel–zinc ferrites. Mater Chem Phys. 2003;82(3):583.

[20] Kader SS, Paul DP, Hoque SM. Effect of temperature on the structural and magnetic properties of $CuFe_2O_4$ nano particle prepared by chemical co-precipitation method. Int J Mater Mech Manuf. 2014;2(1):5.

[21] Nellis WJ, Legvold S. Thermal conductivities and Lorenz functions of gadolinium, terbium, and holmium. Single Crystals Phys Rev. 1969;180(2):581.

[22] Munir A, Ahmed F, Saqib M, Rehman MA. Partial correlation of electrical and magnetic properties of Nd substituted Ni–Zn Nanoferrites. J Magn Magn Mater. 2016;397:188.

[23] Yadav RS, Havlica J, Masilko J, Kalina L, Wasserbauer J, Hajdúchová M, Enev V, Kuřitka I, Kožáková Z. Impact of Nd^{3+} in $CoFe_2O_4$ spinel ferrite nanoparticles on cation distribution, structural and magnetic properties. J Magn Magn Mater. 2016;399:109.

[24] El Moussaoui H. The effects of synthesis conditions on the magnetic properties of zinc ferrite spinel nanoparticles. J Alloys Compd. 2013;581:776.

[25] Zhao L, Yang H, Yu L, Yui C, Zhao X, Yan Y. The studies of nanocrystalline $Ni_{0.7}Mn_{0.3}Nd_xFe_{2-x}O_4$ (x = 0–0.1) ferrites. Phys Lett A. 2004;332(3–4):268.